Nanoparticles for Photoacoustic Imaging of Cancer

Katheryne E. Wilson, Keerthi S. Valluru, and Jürgen K. Willmann

1 Introduction

In this chapter, we present the basics of photoacoustic imaging with an overview of the types of nanoparticles specifically used in the detection of cancer drawing from our own experience and the work of others in the field. Photoacoustic imaging is a highly complementary modality to ultrasound imaging and has potential for several clinical applications [1]. The contrast in photoacoustic imaging is based on optical absorption. Therefore, agent-free photoacoustic imaging visualizes intrinsic tissue chromophores (light absorbing molecules) such as oxygenated and deoxygenated hemoglobin, melanin, and lipid. However, for other applications, such as examining cellular expression of specific cancer markers, the use of exogenous contrast agents is required. Several types of nanoparticles (noble metal, carbon, and mixed composition) have been developed as photoacoustic contrast agents due to their strong optical absorption characteristics. Here, we review some of the notable examples for the various types of nanoparticles for photoacoustic imaging of cancer.

2 Basics of Photoacoustics

The photoacoustic (interchangeably "optoacoustic") effect was first described in 1880 by Alexander Graham Bell when he noticed that sound waves were produced from an absorbing media after being exposed to sunlight transmitted through a rapidly rotating slotted wheel [2]. Furthermore, he noticed that the emitted sound waves changed between different materials and different frequencies of light.

K.E. Wilson, Ph.D. • K.S. Valluru, M.S. • J.K. Willmann, M.D. (✉)
Department of Radiology, School of Medicine, Stanford University,
300 Pasteur Drive, Stanford, CA 94305, USA
e-mail: willmann@stanford.edu

J.W.M. Bulte, M.M.J. Modo (eds.), *Design and Applications of Nanoparticles in Biomedical Imaging*, DOI 10.1007/978-3-319-42169-8_15

These experiments provided the basis upon which modern photoacoustics are built. Formally, the photoacoustic effect is the formation of sound waves after light absorption within a media. For photoacoustic imaging, a pulsed laser is used to irradiate tissues. Upon optical absorption by either an endogenous or exogenous chromophore (a light-absorbing molecule), heat is generated and released to the immediately surrounding environment [3]. This environment undergoes localized, rapid thermal expansion. Upon contraction of the environment to the original state, a high amplitude, broadband acoustic wave is released [4–6]. These transients can be detected using standard ultrasound transducers and reconstruction techniques. As photoacoustic imaging relies on light for generating thermoelastic expansion and the ultrasound transducer for resolution, the method provides optical contrast at depths significantly deeper (up to 7 cm theoretically [5, 6]) than purely optical imaging methods. Furthermore, since optical absorption is dependent on molecular characteristics, the modality can be used as an inherently molecular methodology, which is highly complementary to the anatomical (B-mode) and functional (contrast enhanced and Doppler) imaging provided by clinical ultrasound imaging.

Photoacoustic signal is dependent on the number of photons absorbed and the ability of the media to convert that absorption to heat. Specifically, photoacoustic signal generation can be described as:

$$P = F\mu_a\gamma \tag{1}$$

Where P is the photoacoustic signal intensity, F is the fluence of laser energy in mJ/cm^2, μ_a is the optical absorption coefficient of the absorptive media in cm^{-1}, and γ is the Grüneisen parameter, which describes the heat transfer characteristics of the media. Therefore, photoacoustic signal is linearly dependent on the laser fluence irradiated onto the sample and how absorptive the sample is. Generally, two conditions must be met for the effect to occur, namely thermal and stress confinements. Thermal confinement is met when the duration of the light pulse is shorter than the thermal relaxation time of the media, meaning the pulse duration must be shorter than the time it takes for the heat generated by absorption to dissipate. Stress confinement is met when the pulse duration is shorter than the stress relaxation time. Most laser pulses less than 10 ns will fulfill these requirements for photoacoustic imaging purposes.

2.1 Spectroscopic Photoacoustic Imaging

In biological tissue, the dominant optical absorber is hemoglobin in its two oxygenation states (see Fig. 1). As photoacoustic imaging contrast is highly dependent on optical absorption, this implies photoacoustic imaging is inherently suited for imaging blood. Several applications take advantage of this property such as imaging of tumor neoangiogenesis, monitoring antiangiogenic therapy, and imaging of ischemic events, to name a few [7–11]. However, examining other endogenous or

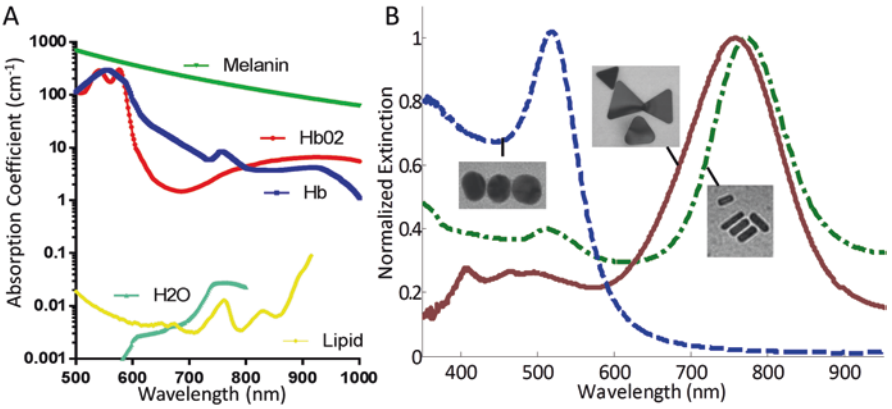

Fig. 1 Optical absorption of endogenous chromophores and exogenous nanoparticle contrast agents. (**a**) Absorption coefficients of several endogenous tissue chromophores. Melanin has the strongest optical absorption, but only occurs in the skin, and therefore hemoglobin in its two oxygenation states (HbO2—oxygenated hemoglobin, and Hb—deoxygenated hemoglobin) dominates photoacoustic images over lipid and water imaging. These spectra have local minimums in the 700–900 nm range, where (**b**) various nanoparticles have tunable peaks in their optical absorption including silver nanoplates (*brown line*) and gold nanorods (*green line*). Nanospheres (*blue line*) act as precursor nanoparticles to synthesize anisotropic shapes

exogenous absorbers beyond hemoglobin states, which is crucial to expand the cancer imaging application of photoacoustic imaging, can result in low signal to background ratios, as optical absorption of hemoglobin will dominate the photoacoustic signal production. One solution is to compare pre- and post-injection images of contrast agents to display signal only corresponding to the exogenous agents. However, using subtraction of images to remove background hemoglobin signal is prone to error due to physiological changes including tumor growth, changes in blood flow, and experimental setup, including laser fluence variations and imaging plane shifts [12]. Therefore, methods are needed to overcome these challenges and minimize background signal from hemoglobin when examining other endogenous or exogenous agents.

Spectroscopic photoacoustic imaging can be implemented to reduce the photoacoustic signal from blood and enhance the signal from the desired absorber by modeling images as linear combinations of absorbers. Optical absorption is dependent on the wavelength of light and the concentration of the photoabsorber. The absorption coefficient $\mu_a(\lambda,r)$, which is dependent on the wavelength "λ" and the spatial position "r," is defined as the product of the molar extinction coefficient ($\mathcal{E}$) and the concentration (C) of the photoabsorber as described [12, 13], providing the following Eq. (2):

$$\mu_a(\lambda,r)=C_1(r)\varepsilon_1(\lambda)+C_2(r)\varepsilon_2(\lambda)+\ldots C_n\varepsilon_n(\lambda) \tag{2}$$

Assuming the optical absorption that provides photoacoustic signal is proportional to the sum of the n photoabsorbers within the imaging plane, the localized absorption coefficient μ_a can be considered as the sum of the "n" individual absorption coefficients. Therefore, if at least "n" wavelengths are used to image a given plane, regression methods can be used to determine the relative concentrations of the "n" photoabsorbers in relative but arbitrary units within the region-of-interest based on the assumption that the photoacoustic signal (known variable as measured in the experiment) is proportional to the molar extinction coefficient "$\mathcal{E}$" (a known variable from the literature [14, 15]) times the concentration "C" of the individual photoabsorbers (unknown variable). The power of the regression improves with additional wavelengths and/or those that represent salient spectral characteristics of the photoabsorbers [13]. The method is most accurately applied when examining a mixture of photoabsorbers that have (1) relatively good optical absorption with hemoglobin being the standard; (2) distinctive spectral characteristics such as sharp peaks; and (3) absorption spectra that are highly distinguishable from each other.

2.2 *Label Free Spectroscopic Photoacoustic Imaging in Cancer*

Endogenous or label-free photoacoustic imaging, involves the examination of intrinsic tissue constituents such as hemoglobin, lipid, melanin, and water, which can be selectively imaged using spectroscopic photoacoustic imaging due to their strong absorption characteristics in the near infrared light region [15–19]. In cancerous tissue, angiogenesis leads to formation of new vasculature, thereby contributing to significant changes in concentration of hemoglobin within the tissue compared to healthy tissue with a subsequent increase in photoacoustic imaging signal [20, 21]. A multitude of studies taking advantage of intrinsic photoacoustic imaging contrast obtained from differences in the absorption spectra of tissue absorbers, such as oxygenated and deoxygenated hemoglobin, have been reported in the literature [22–27]. In a recent study [28], it has been demonstrated that as many as four different breast histologies, including normal ($n=82$), hyperplasia ($n=12$), ductal carcinoma in situ or DCIS ($n=96$), and invasive breast carcinoma ($n=61$), can be differentiated with reasonable accuracy based on the photoacoustic imaging contrast obtained from oxygen saturation, total hemoglobin, and lipid content in a transgenic mouse model (27 mice, $n=251$ mammary glands). With the help of a multiparametric analysis, it was shown that oxygen saturation performed best to differentiate clinically nonactionable (normal/hyperplasia) versus clinically actionable (DCIS and invasive breast carcinoma) findings. Furthermore, a reduction in lipid content was seen as the fat tissue being progressively replaced by a solid tumor during breast cancer development. However, the total hemoglobin was observed to be lower in DCIS and invasive breast carcinoma compared to normal and hyperplasic mammary glands in that study despite the general increase of vascularity in tumors. Therefore, due to complex biological processes, elucidating information concerning disease state based on those parameters only may be challenging.

Also, in instances where the blood vessels are still smaller compared to the detection sensitivity of the photoacoustic imaging system, which might often be the case in the early stages of cancer development, the intrinsic endogenous contrast may not be sufficient to detect any changes between cancer and surrounding healthy tissue. Moreover, not all cancers behave similarly, making it hard to estimate the type of change one might expect from the endogenous absorbers. For instance, will the concentration of lipid in cancer be more, or less compared to healthy tissue? Will different types of cancer show similar traits in absorption? Furthermore, the photoacoustic image contrast obtained from endogenous absorbers is not specific to the cancer or any other disease and may not be sufficient to provide a definitive diagnosis. As such, exogenous contrast agents, which can be synthesized to achieve a desired absorption, can be helpful in increasing the sensitivity and contrast-to-noise of photoacoustic imaging for cancer imaging. In addition, exogenous photoacoustic imaging agents, such as nanoparticles, that can interact with the tissue or bind to a cancer-specific biomarkers can also improve specificity, thereby allowing molecular imaging capabilities.

3 Nanoparticles for Photoacoustic Cancer Imaging

Nanoparticles are well suited for use as contrast agents, as their size is on scale with biological processes and cells, allowing visualization of the intricate processes that occur. These small sizes allow enhanced optical absorption, biodistribution, and clearance properties that can all be fine-tuned for specific applications. In the following sections, a brief introduction on general synthesis and bioconjugation methods of nanoparticles will be presented followed by key examples of use for photoacoustic imaging of cancer.

3.1 Plasmonic Noble Metal Nanoparticles

Plasmonic noble metal (e.g., gold, silver) nanoparticles constitute the most commonly researched probes for photoacoustic imaging of cancer. These particles have relatively facile and rapid (a few hours) synthesis methods with tunable size and shape parameters to allow for application-specific optimization of absorption properties that provide sharp absorption peaks within the near infrared tissue "optical window," where endogenous tissues absorption is dominant otherwise. Furthermore, noble metal nanoparticles are easily bioconjugated to targeting moieties. However, in the case of gold nanoparticles, while they have little interaction with biological systems preventing toxicity, they are often retained in the liver and spleen. In the case of silver, which does degrade in biological environments, there is concern of potential silver toxicity. Current research is focused on overcoming these limitations because the per particle optical absorption tends to be higher in noble metal nanoparticles compared to any carbon nanotubes, polymer, or dye based nanoparticles due to the interesting phenomenon of plasmon resonance, making them promising contrast agents for photoacoustic imaging of cancer.

3.2 Plasmon Resonance

Nanoscale particles have many interesting properties that the same materials in bulk do not. One of the main reasons for this is the shift in the ratio of surface atoms to interior atoms. Surface atoms interact with the surrounding environment while interior atoms do not. This increased interaction with the environment gives rise to the superior optical absorption of noble metal nanoparticles because of surface plasmon resonance (SPR) [29–31]. Concretely, free electrons in metals are able to travel throughout the material, and in nanoscale particles, they do so free of scattering as the mean free path is greater than the size of the nanoparticle. Therefore, when an electromagnetic wave front with a wavelength larger than the diameter of the particle passes, the free electron cloud is polarized to the sides of the nanoparticle depending on the oscillating charge of the wave, resulting in coherent resonation at the same frequency. The size, shape, and surface environment of the nanoparticle all alter the SPR resonance (absorption) peaks, allowing nanoparticles to be finely tuned to specific applications in the visible and near infrared regions [29–31]. Once noble metal nanoparticles have the desired absorption characteristics, it is important to fine tune the pharmacokinetics and distribution for an optimal imaging system.

3.3 Bioconjugation

Due to their small size, unconjugated nanoparticles can be directly used as cancer contrast agents through the "enhanced permeability and retention effect" (EPR) which typically allows up to 5 % of the injected dose to accumulate nonspecifically within tumor tissues [32]. In tumors, the recruitment and growth of new blood vessels to supply nutrients occurs more quickly than typical angiogenesis [20]. Therefore, the organization and function of these rapidly grown vessels is abnormal, including poorly aligned endothelial cells, which leave large gaps of up to 800 nm in diameter between cells. Combined with ineffective lymphatic drainage, these factors make nanoparticles more likely to accumulate within tumor tissue compared to normal tissue [33, 34]. However, the efficiency of nanoparticle delivery using the EPR effect is highly variable between and within cancer types and stages, and is increased in preclinical xenograft tumor models due to a faster tumor development rate compared to native cancers [33]. Therefore, it is advantageous to conjugate molecular targets (such as antibodies, antibody fragments, peptides, aptamers, or metabolites [35]) to the surface of nanoparticles to, for example, increase receptor-mediated endocytosis into tumor cells or to allow for photoacoustic molecular imaging of a specific biomarker of the tumor vasculature. While other binding motifs (i.e., hydrophobic, electrostatic interactions, and van der Waals forces [36]) can be used to attach biomolecules to the surface of nanoparticles, covalent binding between SH, O, or N atoms through their unshared election pairs are preferred for clinical applications due to an increase in the stability of the constructs [36].

One of the typically leveraged bonds is the metal–thiol covalent bond mediated through sulfhydryl (SH) functional groups in thiols (R-SH), which is almost as strong as the gold–gold (Au–Au) bond, though the exact mechanism is still being elucidated [37, 38]. For bioconjugation purposes, the thiol interaction allows binding with cysteine amino acid residues, which have a thiol functional group allowing for direct protein conjugation. However, the number of cysteines can be limited or nonexistent in proteins, and therefore, proteins containing -NH2 groups (typically the more abundant lysine residue, occasionally arginine) could be attached by conversion to SH groups through EDC (1-ethyl-3-(3-dimethylaminopropyl) carbodiimide) or sulfo-NHS chemistry [35]. These reactions are fairly straightforward and short in duration up to a couple of hours [35]. Finally, to avoid a rapid immune response and clearance of nanoparticles triggered by nonspecific protein absorption on the surface, increased circulation time, and increased serum solubility [39], nanoparticles are typically coated with polyethylene glycol (PEG, PEGylation) using commercially available PEG-SH.

3.4 Gold Nanoparticles

Gold nanoparticles are by far the most commonly used plasmonic noble metal nanoparticle for photoacoustic imaging of cancer. Gold nanoparticles are bioinert in terms of cytotoxicity, but accumulate within the mononuclear phagocyte system [40], including the spleen, liver, and lymphatic system for up to 2–6 months (the final time point in several studies [41]); therefore, clinical use of gold nanoparticles remains elusive, as it requires more extensive biosafety and evaluation standards to elucidate whether this accumulation poses health risks, which is currently unclear. Extensive research has been dedicated to synthesizing monodisperse gold nanoparticles in a variety of sizes and shapes (spheres, rods, cubes, plates, barbells, rice, tetrapods, etc. see Fig. 2 [28, 42–44]), which allows fine-tuning of optical absorption properties for applications of photoacoustic imaging of cancer.

3.4.1 Synthesis

While “top-down” approaches (starting with bulk gold and removing material until nanoparticles remain) exist for synthesis of gold nanoparticles, “bottom-up” approaches (building nanoparticles from reduced metal ions) have become sufficiently optimized to produce relatively monodisperse particles in bulk and will be the focus here. One common method for gold nanosphere production involves reduction of gold(III) derivatives, such as $HAuCl_4$, using a weak reducing agent such as citric acid [45, 46]. The ratio of the reducing agent to the salt and reducing time determine the size of the nanoparticles, which are citrate stabilized in the solution. Particles can then be surface capped through PEGylation for purification and used for in vivo applications. Synthesis of anisotropic nanoparticles, most notably

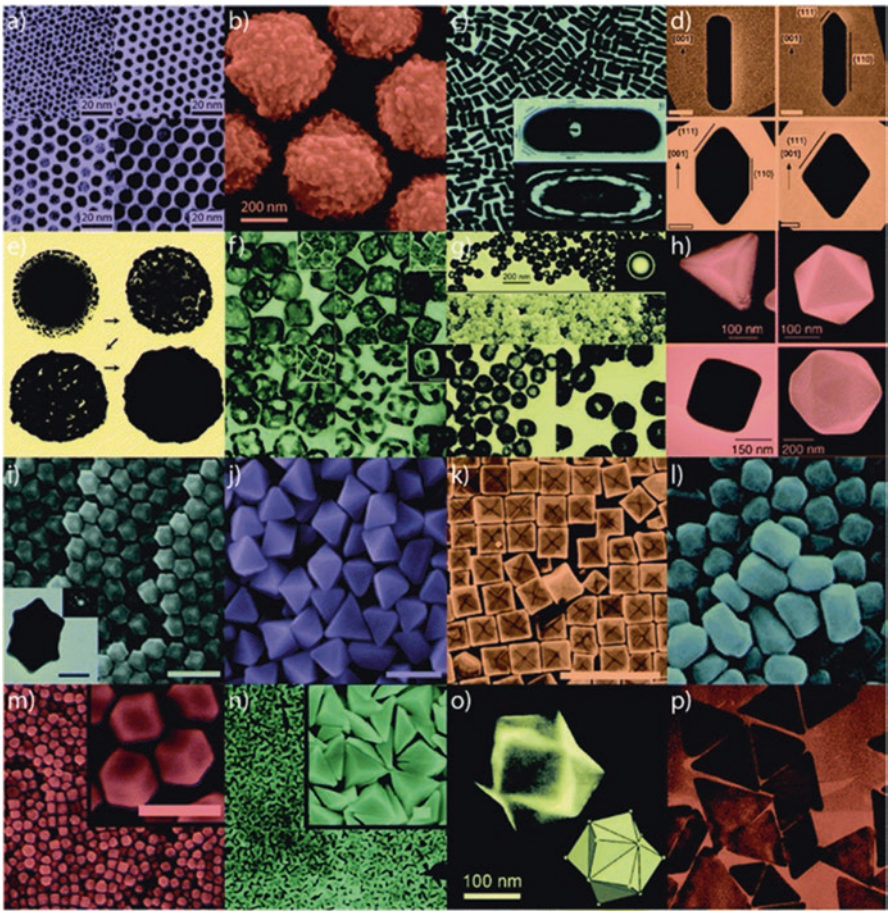

Fig. 2 Gold nanoparticles of various size and shape with potential applications in biomedicine. Small (**a**) and large (**b**) nanospheres, (**c**) nanorods, (**d**) sharpened nanorods, (**e**) nanoshells, (**f**) nanocages/frames, (**g**) hollow nanospheres, (**h**) tetrahedra/octahedra/cubes/icosahedra, (**i**) rhombic dodecahedra, (**j**) octahedra, (**k**) concave nanocubes, (**l**) tetrahexahedra, (**m**) rhombic dodecahedra, (**n**) obtuse triangular bipyramids, (**o**) trisoctahedra, and (**p**) nanoprisms [44]—Reproduced by permission of The Royal Society of Chemistry

nanorods, begins with a similar method but using stronger reducing agents, (such as sodium borohydride) to produce small gold nanospheres (~4 nm). These small spheres act as "seeds" onto which carefully controlled epitaxial gold ion deposition is continued through the use of selective growth restriction surfactants that bind to faces of the seed with preferential crystal structures and atom spacing. In the case of gold nanorods, cetyltrimethylammonium bromide (CTAB) is used in combination with silver nitrate to block gold deposition on the {111} or {100} side faces, leaving the {110} common axis faces free for anisotropic growth {denote atomic crystal lattice structures} [47]. Similar to spheres, nanorods, and other anisotropic shapes

can be stabilized through PEGylation for in vivo applications. Many other shapes (see Fig. 2) can be synthesized by varying synthesis parameters including temperature, component ratios, and surfactants. Using these synthesis methods combined with bioconjugation of targeting moieties allows fine tuning of nanoparticle composition for specific applications of photoacoustic imaging of cancer.

3.4.2 Applications

The use of nanoparticles as contrast agents for photoacoustic imaging of cancer currently remains in the preclinical research stage, though several interesting studies have been explored. For example, gold nanorods have been used to image multiple types of cancers. Jokerst et al. [48] demonstrated the use of gold nanorods to image three types of ovarian cancer tumors: 2008, HEY, and SKOV3 subcutaneously grown in mice ($n=3$). They reported a 2.3-fold photoacoustic signal increase with intratumoral injection and a 3.5-fold increase with intravenous injection of gold nanorods at excitation wavelength of 756 nm respectively. The work by Zhong et al. [49] further demonstrates the applicability of gold nanorods beyond imaging, as they reported photoacoustic therapy using gold nanorods conjugated with folic acid in mice bearing HeLa (human cervical cancer) tumors that overexpress folate receptor. Folic acid conjugation allows the nanoparticles to bind to folate receptor whose expression is minimal in healthy tissues and high in cancers such as lung, breast, kidney, brain, cervix, or ovary cancer [50, 51]. Photoacoustic therapy although similar in principle to photoacoustic imaging, destructs individual target cells with laser-induced shock waves. When a photoabsorber is irradiated with a pulsed laser, the optical energy is transformed into mechanical energy, resulting in a shock wave without the side effect of heating or cavitation [52]. In photoacoustic therapy, the generation of shock waves rely on the efficiency of photoabsorbers to convert light energy into acoustic energy, with suitable candidates reported as indocyanine green containing nanoparticles (ICG-PL-PEG), single-walled carbon nanotubes, and gold nanorods [49, 53, 54]. When compared with images of mice injected with folic acid conjugated single-walled carbon tubes, and unconjugated gold nanorods, the tumor growth rate in mice treated with folic acid-conjugated gold nanorods was observed to be significantly lower over a duration of 24 days after treatment.

Another type of gold nanoparticles, nanoshells, have been used to study colon cancers. Li et al. [55] reported the intravenous use of PEGylated gold nanoshells in mice bearing CT26.wt colon cancer tumors grown subcutaneously. When imaged for 6 h using photoacoustic microscopy, the gold nanoshells were seen to be progressively taken up by the tumor foci, while those in the vessels were cleared out, indicating an enhancement in photoacoustic signals with a contrast ratio of 6.5 between the tumor foci to the vessels. Li et al. [56] reported the use of gold nanocages for photoacoustic imaging of cerebral cortex, sentinel lymph nodes, and melanoma in small animals. When gold nanocages were injected in rats to study their brain cortex [57], 81 % enhancement in blood absorption was reported over the intrinsic contrast. In a similar study conducted in rats to image sentinel lymph nodes [58], a gradual accumulation

of gold nanocages was observed leading to a gradual increase in photoacoustic signal 28 min after injection. Likewise, gold nanocages functionalized with [Nle^4, D-Phe^7]-α-melanocyte-stimulating hormone were used for active targeting and resulted in a 300 % higher photoacoustic signal enhancement because of ligand-receptor binding on melanoma cells in mice compared to PEGylated gold nanocages 6 h after injection [59]. In a recent study by Shujing et al. [60], molecular imaging and photoacoustic therapy of gastric cancer stem cells using bioconjugated gold nanostars was reported. Gold nanostars conjugated with CD44v6 monoclonal antibody were intravenously injected in orthotopic and subcutaneous mice tumor models of human gastric cancer. Their results suggest that the bioconjugated gold nanostars successfully targeted the gastric vascular system at 4 h after injection resulting in 250 % increase in photoacoustic signal compared to the signal acquired from mice injected with unconjugated PEGylated gold nanostars. Moreover, tumor growth inhibition was also reported with an extension of survivability of tumor bearing mice.

Furthermore, introduction of gold nanospheres into a biological environment leads to complex interactions, such as aggregation of nanoparticles within cells, which can be visualized due to the resulting change in optical absorption spectra. Mallidi et al. [61] reported the synthesis and application of bioconjugated gold nanospheres (20 nm dia.) that can specifically bind to the cancer biomarker endothelial growth factor receptor (EGFR) for improved differentiation of cancer from background healthy tissue. EGFR-expressing human epithelial carcinoma cells (A431, $n=6$) and EGFR-negative human breast cancer cells (MDA-MB-435, $n=3$) were subcutaneously inoculated in mice followed by intravenous injection of EGFR-targeted or PEGylated gold nanospheres. Results of EGFR-targeted gold nanoparticles in A431 tumors are shown in Fig. 3a, b. A wavelength shift in the

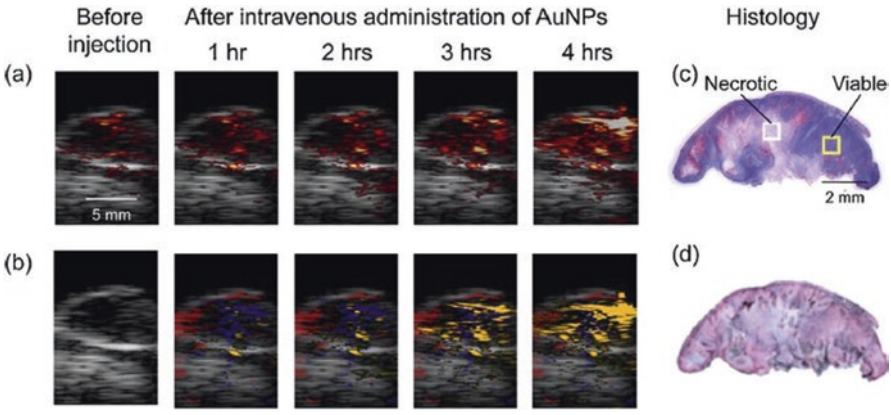

Fig. 3 Gold nanoparticles for photoacoustic imaging of cancer. (**a**) Photoacoustic and (**b**) multi-wavelength spectroscopic photoacoustic images pseudo-colored to show oxygenated- (*red*) and deoxygenated hemoglobin (*blue*), and accumulation of gold nanoparticles (*yellow*) before and 1, 2, 3, and 4 h after intravenous injection of EGFR-targeted gold nanoparticles in a subcutaneous A431 breast cancer tumor. (**c**) H&E and (**d**) silver enhancement staining of histology tumor slices showing accumulation of EGFR-targeted gold nanoparticles within the tumor. Reprinted with permission from [61].

absorption of targeted gold nanospheres in EGFR expressing tumors was observed from 520 nm (green) to 720 nm (near infrared) due to plasmon resonance coupling. Effectively, cellular internalization and aggregation of nanoparticles into lysosomal compartments brings nanoparticle, and their individual free electron clouds, into close proximity. This grouping of nanoparticles then acts as a larger nanoparticle of a different shape with one associative electron cloud that has a distinct resonance frequency and associated optical absorption, changing the overall absorption spectrum from that of individual nanoparticles. Accumulation was confirmed by silver staining (which detects the presence of noble metals by depositing ionic silver until the nanoparticle can be visualized with light microscopy) of histological sections, along with an increase in photoacoustic signal over time (4 h after injection) shown in Fig. 3c, d. In contrast, images of mice with PEGylated gold nanospheres showed no significant change in photoacoustic signals, indicating that using targeted nanoparticles increased specificity in imaging EGFR-expressing cancer cells.

Overall, gold nanoparticles have been extensively used as contrast agents for photoacoustic imaging due to their excellent optical absorption and finely tunable absorption characteristic that can be optimized for specific applications. However, the bioaccumulation of gold nanoparticles remains a limiting factor in their use clinically.

3.5 Silver Nanoparticles

Silver nanoparticles have been commonly used in biomedical and cosmetic purposes for their antibacterial properties [62]. Unlike gold nanoparticles, silver nanoparticles dissolve over time in biological environments making them more suitable for repeat administrations for clinical purposes compared to gold nanoparticles [62]. However, the ability of silver nanoparticles to degrade introduces new challenges for their biomedical use, including potential silver toxicity [63] through the introduction of reactive oxygen species leading to cellular oxidative stress and lipid peroxidation [64] and decreased stability which would affect their desired optical absorption characteristics.

3.5.1 Synthesis

Silver nanoparticles are synthesized very similarly to gold nanoparticles, predominantly through seed-mediated growth procedures. Reducing agents appropriate for silver particles include hydrazine, ascorbic acid, temperature increases, and light exposure. Silver seeds approximately 3 nm in diameter can be synthesized by the reduction of silver nitrate ($AgNO_3$) using sodium citrate and adding sodium borohydride ($NaBH_4$) in a dropwise fashion, followed by stabilization by bis(p-sulfonatophenyl)phenylphosphine dihydrate dipotassium (BSPP) [65]. The further growth on anisotropic shapes is accomplished similarly to that of gold nanoparticles through the addition of silver salts and reducing agents [66].

3.5.2 Applications

The use of silver nanoparticles for photoacoustic imaging of cancer has been more limited due to potential silver toxicity concerns and stability issues. However, some groups have been able to overcome these challenges by using a specific type of silver nanoparticles for imaging of pancreatic cancer xenografts. Homan et al. [66] demonstrated the synthesis of biostable sliver nanoplates (edge-length: 60.9 nm, thickness: 12.5 nm) by functionalizing them with thiol terminated methoxy-polyethylene glycol (mPEG-SH). They reported the application of PEG-passivated silver nanoplates conjugated to a monoclonal antibody to EGFR (a-EFGR) in detecting orthotopic human pancreatic cancer xenografts grown in mice. At first, cancer binding specificity of a-EFGR conjugated sliver nanoplates (SPR peak: 800 nm) was confirmed in vitro by incubating EGFR-expressing pancreatic cancer cells in three conditions: with no nanoplates, PEGylated nanoplates, and a-EGFR conjugated nanoplates, with only the last group showing any uptake. Further incubation of three different cell lines: MPanc96 (EGFR-expressing pancreatic cancer), L3.6pl (EGFR-expressing pancreatic cancer), and HPNE (non-cancerous pancreatic cells) in vitro for 24 h confirmed no cytotoxicity up to concentrations of 1 mg/mL silver nanoplates. Spectroscopic photoacoustic imaging of orthotopic pancreatic mice models up to 6 h after intravenous injection of a-EGFR conjugated nanoplates showed a heterogeneous accumulation of nanoplates in the tumor, which was also confirmed later by silver staining of histological slices, indicating that silver nanoparticles can increase the tumor contrast over surrounding tissue. Homan et al. [67] have also demonstrated an enhancement of photoacoustic imaging contrast in porcine pancreatic tissue ex vivo using another group of sliver nanoparticles called silver nanocages in a study aimed to further improve pancreatic cancer detection. The silver nanocages constitute silica nanospheres (180–520 nm) coated with a porous layer of sliver (5–60 nm) and the authors reported the possibility of using them beyond imaging for targeted drug delivery if the silica core material were to be replaced with a suitable drug-eluting material. Overall, silver nanoparticles remain a promising contrast agent for photoacoustic imaging assuming potential toxicity and stability issues can be sufficiently addressed.

3.6 Silica Coating of Noble Metal Nanoparticles

While, noble metal nanoparticles have excellent optical absorption abilities, optical absorption ultimately leads to instability of the nanoparticles after longer term imaging. Upon pulsed laser irradiation, optical absorption is converted to heat. Nanoscale particles tend to have lower melting temperatures due to the increase in ratio of surface to bulk atoms. Therefore, after prolonged imaging, anisotropically shaped noble metal nanoparticles tend to melt into more energy efficient shapes, such as spheres, altering their optical absorption peaks. Coating these particles with silica not only increases stability for prolonged or longitudinal imaging, but also provides an amplification of the photoacoustic signal due to an increase in the interfacial heat transfer between the particle and the surrounding environment. To produce silica-coated

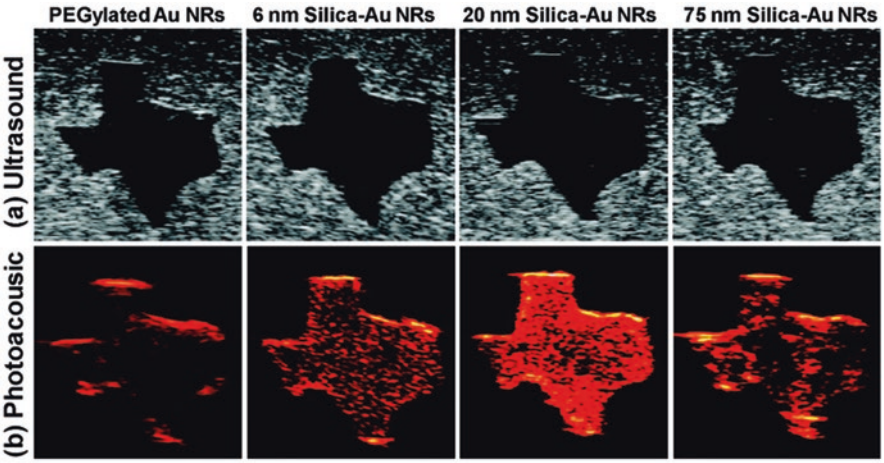

Fig. 4 (**a**) Ultrasound and (**b**) photoacoustic images (*top* to *bottom*) of inclusions containing the same number of (I) PEGylated gold nanorods and gold – silica core – shell nanorods with (II) 6 nm silica coating, (III) 20 nm silica coating, and (IV) 75 nm silica coating (left to right). Each image covers a 6 mm by 6 mm field of view. Reprinted with permission from Ref. [3]

metal nanoparticles, silica is deposited onto preprepared and PEGylated nanoparticles via the Stöber method[68]. Tetraethyl orthosilicate (TEOS) usually acts as the source of silica and the reaction is completed in an alcohol and ammonia solution [68]. The surface of silica nanoparticles can be conjugated using alkane silanes [36].

Chen et al.[3, 68] reported the development and implementation of gold nanorods coated with silica of varying thickness: 6, 20, and 75 nm for photoacoustic imaging of tissue-mimicking phantoms. When compared with signals from PEGylated gold nanorods without silica, the 20 nm silica-coated gold nanorods demonstrated the highest fold (3.8 times) increase in photoacoustic signals. The larger 75 nm silica-coated gold nanorods were reported to show a reduced photoacoustic signal (only 2.3 times higher than PEGylated) than 20 nm silica-coated nanorods, possibly due to reduced local fluence, as a consequence of increased scattering as shown in Fig. 4. Moreover, the silica-coated nanorods were reported to exhibit superior stability than PEGylated nanorods under high-fluence laser pulses. Overall, silica-coating presented a slight shift in wavelength towards the red without altering the optical absorption of gold nanoparticles increasing the usefulness of gold nanoparticles as photoacoustic imaging contrast agents through increase in stability and signal amplification.

3.7 Carbon Nanotubes

Carbon nanotubes (CNT) are graphene sheets that have been rolled into cylinders that have extremely long aspect ratios (>100) as diameters are typically a few nanometers or less and lengths up to hundreds of nanometers. CNTs have excellent stability and interesting semiconductor and optical absorption properties, and their functions in biomedical applications are currently being explored.

3.7.1 Synthesis

Carbon nanotubes represent a more challenging nanoparticle to synthesize requiring extremely high temperatures and specialized equipment. However, they are commercially available for those who would like to use them for biomedical research without large startup costs. The three main methods of carbon nanotube synthesis include arc-discharge, laser ablation, and chemical vapor deposition [68]. Arc-discharge and laser ablation are "top-down" approaches, where bulk carbon sources are vaporized at thousands of degrees Celsius into high-quality carbon nanotubes intermixed with large amounts of byproduct. The "bottom-up" approach uses small metal seeds to initiate growth through chemical vapor deposition at much lower temperatures between 500 and 1000 °C [69]. The optical absorption of CNTs is high with a very broad absorption over the visible and near infrared regions. Carbon nanotubes are hydrophobic after synthesis and, therefore, need surface modification to be compatible with biological systems. When sonicated with PEG-phospholipid compounds, the hydrophobic tails of the phospholipids interact strongly with the walls of the carbon nanotubes, leaving the PEG to interact with the aqueous solution [69, 70]. Furthermore, function linkers can be used in lace of the PEG to allow for conjugation of biologic targeting moieties. However, even after surface modification, there are concerns over cytotoxicity of the CNTs. Specifically, the concerns relate to how shapes with extremely high aspect ratios interfere with cellular endocytosis and cells physically cannot fully engulf objects of this shape [71]. However, CNTs have been used in preclinical cancer models.

3.7.2 Applications

In one such application, Zerda et al. [70] reported an eightfold increase in the photoacoustic signal in mice bearing U87MG glioblastoma tumors overexpressing $\alpha_v\beta_3$ integrin upon tail-vein injection of single-walled CNTs conjugated with cyclic RGD peptides targeting $\alpha_v\beta_3$ integrin ($n=4$), compared to photoacoustic signals from tumor bearing mice injected with non-targeted PEGylated nanotubes, as shown in Fig. 5. Three-dimensional spectroscopic photoacoustic imaging was performed before and up to four hours after injection of nanotubes followed by tumor extraction for ex vivo analysis using Raman microscope, which reported a fourfold Raman signal increase in mice injected with targeted single-walled CNTs compared to the signal from mice with non-targeted nanotubes validating the photoacoustic results. In another study, Nguyen et al. [72] demonstrated a 20-fold increase in optical absorption and a twofold increase in photoacoustic image contrast in porcine bladder tissue injected with single-walled CNTs conjugated with ICG compared to unconjugated CNTs with implications to improve bladder cancer detection. They reported the possible reasons for disproportion (10:1 ratio) between optical absorption and photoacoustic signal as nonuniform spatial distribution of ICG conjugated CNTs, the inhomogeneous absorbance of CNTs in tissue, and the precision of the mechanical movements of the PA system during signal acquisition.

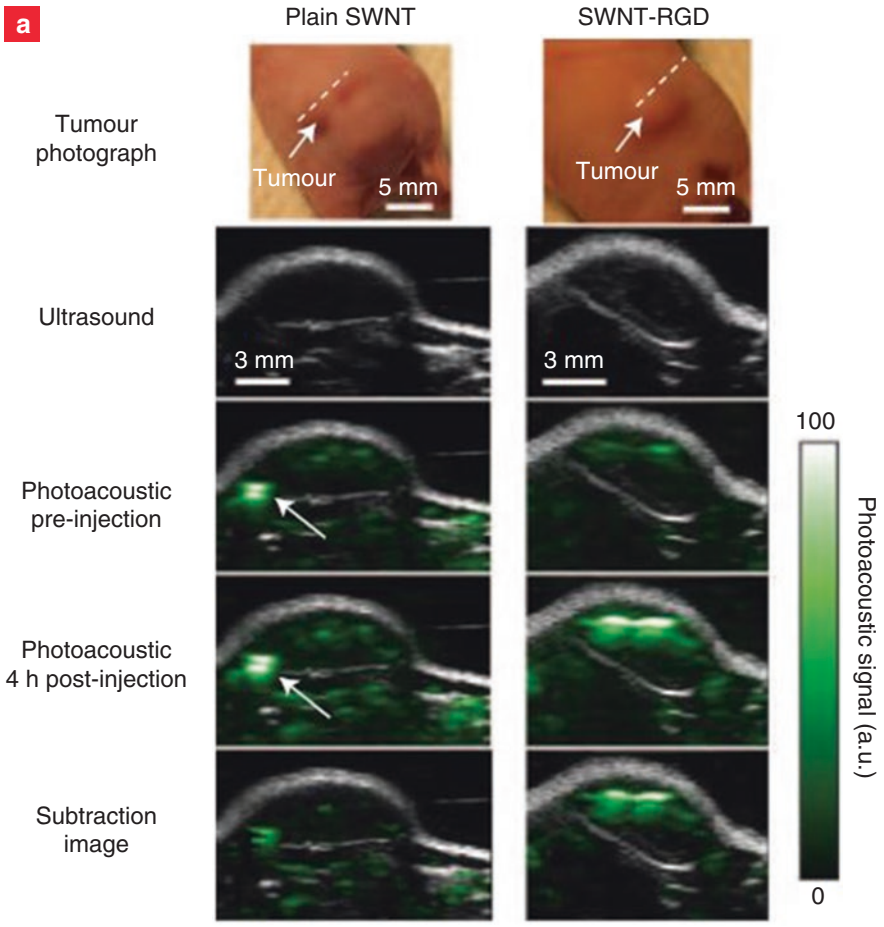

Fig. 5 Carbon nanotubes for photoacoustic imaging of cancer. Ultrasound and photoacoustic images of PEGylated and RGD peptide targeted single walled carbon nanotubes accumulated with an U87MG glioblastoma subcutaneous tumor at 4 h post intravenous injection. Targeted carbon nanotubes show increased tumor accumulation than mice injected with PEGylated carbon nanotubes (four- to sevenfold). Adapted with permission from Ref. [70]

3.8 Mixed Composition Nanoparticles

In order to achieve a complete set of desirable characteristics in nanoparticle contrast agents, including strong optical absorption, biocompatibility, appropriate size, shape, surface binding capabilities, and clearance rates, mixed composition nanoparticles have been explored. Typically, these particles comprise of a "carrier" of either polymer or biocompatible scaffold and a "payload" of optically absorbing media, either dyes or smaller nanoparticles for photoacoustic signal generation. For example, in the work by Zhong et al. [53], synthesis of indocyanine green (ICG) and

phosopholipid-polyethylene glycol (ICG-PL-PEG) nanoparticles was reported with a demonstration of photoacoustic image contrast enhancement upon injection into the flank region of female Balb/c mice. With all the individual components of ICG-PL-PEG nanoparticles already approved by FDA for human use, these composite dye-based nanoparticles have a higher potential of clinical translation. The authors have later modified these ICG-PL-PEG nanoparticles by combining with folic acid and reported their use as cancer-targeting nanoprobes suggesting a reduced tumor growth after photoacoustic therapy [54].

Mixed composition nanoparticles also offer the potential for dual contrast enhancement for photoacoustic imaging and another imaging modality, typically ultrasound. Nanodroplets are an exciting field of research for dual contrast enhancement for combined ultrasound and photoacoustic imaging. Nanoscale (200 nm diameter) droplets of perfluoropentane encapsulated with a biocompatible bovine serum albumin shell in which gold nanorods (40 nm) were suspended, act as both photoacoustic contrast agents (through both thermoelastic expansion and vaporization mechanisms) and ultrasound contrast agents [73]. Upon pulsed laser irradiation, the gold nanoparticles (photoacoustic contrast agents) in the shell undergo thermoelastic expansion, emitting high frequency ultrasound transients, which vaporize the encapsulated liquid perfluoropentane into its gaseous state, converting to bubbles providing contrast for ultrasound thus providing co-registered dual contrast. This theme has been continued by replacing the gold nanorods with other, more clinically translatable optical triggers such as dyes and organic compounds. Jian et al. [74] reported the synthesis of perfluorohexane liquid nanodroplets incorporated with India ink and encapsulated with FDA approved poly-lactic-co-glycolic acid shell capable of undergoing liquid-to-gas phase transition via vaporization upon exposure to optical energy instead of ultrasound exposure. When these nanodroplets were injected intratumorally in MDA-MB-231 tumor bearing mice ($n=5$), photoacoustic signal amplitude post-injection was observed to be 20-fold higher than that of pre-injection. However, the signal enhancement reported was attributed to thermoelastic expansion alone and not phase-transition due to the laser power limitation of their photoacoustic imaging system (800 nm, 1 mJ/cm^2). To further validate the in vivo phase-transition ability of India ink nanodroplets, B-mode and contrast ultrasound imaging was performed on another group of MDA-MB-231 tumor-bearing mice ($n=5$) after exposing the tumors to a high energy laser (532 nm, 12 mJ/cm^2) for 10 s indicating a 20-fold contrast ultrasound signal enhancement post-laser exposure compared to pre-laser exposure. Hannah et al. [75] also showed similar results using ICG dye internalized to the center of the nanodroplets.

Recently, Paproski et al. [76] have synthesized a new class of nanodroplets called porphyrin nanodroplets (diameter of 185 nm) and injected them intratumorally in an HT1080 tumor in the chorioalantoic membrane of a chicken embryo. Porphyrin nanodroplets constitute liquid perfluorobutane core and a phosopholipid-porphyrin shell, which possesses strong optical absorption in the near infrared region making them suitable for photoacoustic imaging. Additionally, upon absorption of optical or ultrasound energy, porphyrin nanodroplets not only undergo phase change into a perfluorobutane gas, but also expand in size to form microbubbles that can provide ultrasound contrast.

They reported that an enhanced visualization of tumor indicating accumulation of porphyrin nanodroplets was observed with spectroscopic photoacoustic imaging throughout or at the periphery of tumor, demonstrating their usefulness in exhibiting the EPR effect. Nanodroplets have been extensively examined in proof-of-principle studies, however substantial extravascular localization in tumors has yet to be achieved leaving advancement into further preclinical animal studies a challenge.

In contrast, Huynh et al. [77] reported the reverse-conversion of porphyrin microbubbles (1–10 μm) into porphyrin nanoparticles (5–500 nm) in situ and demonstrated their applicability as photoacoustic imaging contrast agents in KB (human-epidermoid carcinoma) xenograft-bearing mice. Unlike nanodroplets that have a liquid core, porphyrin nanoparticles constitute a bacteriochlorophyll-lipid shell encapsulating perfluorocarbon gas core (824 nm peak absorbance), the same as their parent microbubbles. The nanoparticle conversion was achieved using a low-frequency, high-duty cycle ultrasound (conversion ultrasound). It was reported that conversion ultrasound ensured the delivery and retention of porphyrin nanoparticles to the tumor site bypassing the EPR, as indicated by the photoacoustic signal from the tumor, which was maintained for at least 2 h compared to the photoacoustic signal that was decreased within 30 min post-injection of porphyrin microbubbles without any conversion. Overall, mixed composition nanoparticles allow for optimization of nanoparticles for photoacoustic and other modalities, by using the optimized characteristics from each component.

4 Conclusions

Nanoparticles have been extensively used for various biomedical imaging purposes including the emerging field of photoacoustic imaging. An overview of current literature has been presented in this chapter along with background, synthesis, and applications of nanoparticles in photoacoustic imaging of cancer. Extensive explorations and reviews of nanoparticles for photoacoustic imaging in cancer can be found in the literature [78–83]. Nanoparticles that are optimized for photoacoustic imaging vary in size, shape, form, and material, but serve a common purpose of enhancing the image contrast by interacting with the tumor via enhanced permeability and retention effect either intrinsically or through surface modifications and bioconjugation with targeting moieties. Although they present excellent advantages over endogenous imaging, clinical adoption of nanoparticles has been limited due to remaining concerns over cytotoxicity and biodegradability, and the inability to accumulate sufficiently and homogenously within tumors. However, in order to leverage the molecular imaging capabilities of photoacoustic imaging and improve the diagnostic and prognostic rates of cancer detection, new classes of contrast agents that can retain their imaging benefits while minimizing the hazards, are necessary. Ongoing research explores the development and implementation of nanoparticles that constitute one or more materials, which are already FDA approved to support the eventual successful clinical translation of this promising new imaging approach.

References

1. Valluru KS, Wilson KE, Willmann JK. Photoacoustic imaging in oncology: translational preclinical and early clinical experience. Radiology. 2016;280(2):332–49.
2. Bell AG. Production of sound by radiant energy. J Franklin Inst. 1881;111(6):401–26.
3. Chen Y-S, Frey W, Kim S, Kruizinga P, Homan K, Emelianov S. Silica-coated gold nanorods as photoacoustic signal nanoamplifiers. Nano Lett. 2011;11(2):348–54.
4. Diebold GJ, Sun T, Khan MI. Photoacoustic monopole radiation in one, two, and three dimensions. Phys Rev Lett. 1991;67(24):3384–7.
5. Wang L V., Wu H-I, Masters BR. Biomedical optics, principles and imaging. J Biomed Opt. Wiley-Interscience; 2008.
6. Beard P. Biomedical photoacoustic imaging. Interface Focus. 2011;1(4):602–31.
7. Siphanto RI, Thumma KK, Kolkman RGM, Van Leeuwen TG, De Mul FFM, Van Neck JW, et al. Serial noninvasive photoacoustic imaging of neovascularization in tumor angiogenesis. Opt Express. 2005;13(1):89–95.
8. Pan D, Pramanik M, Senpan A, Allen JS, Zhang H, Wickline SA, et al. Molecular photoacoustic imaging of angiogenesis with integrin-targeted gold nanobeacons. FASEB J. 2011;25(3):875–82.
9. Flogel U, Ding Z, Hardung H, Jander S, Reichmann G, Jacoby C, et al. In vivo monitoring of inflammation after cardiac and cerebral ischemia by fluorine magnetic resonance imaging. Circulation. 2008;118(Copyright (C) 2011 U.S. National Library of Medicine.):140–8.
10. Wang B, Karpiouk A, Yeager D, Amirian J, Litovsky S, Smalling R, et al. In vivo intravascular ultrasound-guided photoacoustic imaging of lipid in plaques using an animal model of atherosclerosis. Ultrasound Med Biol. Elsevier; 2012.
11. Brannon-Peppas L, Blanchette JO. Nanoparticle and targeted systems for cancer therapy. Adv Drug Deliv Rev. 2004;56(11):1649–59.
12. Kim S, Chen Y-S, Luke GP, Emelianov SY. In vivo three-dimensional spectroscopic photoacoustic imaging for monitoring nanoparticle delivery. Biomed Opt Express. 2011;2(9):2540–50.
13. Luke GP, Nam SY, Emelianov SY. Optical wavelength selection for improved spectroscopic photoacoustic imaging. Photoacoustics. 2013;1(2):36–42.
14. Prahl S. Optical Properties Spectra. 2001.
15. Jacques SL. Optical properties of biological tissues: a review. Phys Med Biol. 2013;58(11):R37–61.
16. Guggenheim JA, Allen TJ, Plumb A, Zhang EZ, Rodriguez-Justo M, Punwani S, et al. Photoacoustic imaging of human lymph nodes with endogenous lipid and hemoglobin contrast. J Biomed Opt. 2015;20(5):050504.
17. Dogra VS, Chinni BK, Valluru KS, Joseph JV, Ghazi A, Yao JL, et al. Multispectral photoacoustic imaging of prostate cancer: preliminary ex-vivo results. J Clin Imaging Sci. 2013;3:41.
18. Ermilov SA, Khamapirad T, Conjusteau A, Leonard MH, Lacewell R, Mehta K, et al. Laser optoacoustic imaging system for detection of breast cancer. J Biomed Opt. 2009;14(2).
19. Allen TJ, Hall A, Dhillon AP, Owen JS, Beard PC. Spectroscopic photoacoustic imaging of lipid-rich plaques in the human aorta in the 740 to 1400 nm wavelength range. J Biomed Opt. 2012;17(6):612091–6120910.
20. Weis SM, Cheresh DA. Tumor angiogenesis: molecular pathways and therapeutic targets. Nat Med. 2011;17(11):1359–70.
21. Alameddine RS, Hamieh L, Shamseddine A. From sprouting angiogenesis to erythrocytes generation by cancer stem cells: evolving concepts in tumor microcirculation. Biomed Res Int. 2014;2014:1–8.
22. Wang X, Xie X, Ku G, Wang LV, Stoica G. Noninvasive imaging of hemoglobin concentration and oxygenation in the rat brain using high-resolution photoacoustic tomography. J Biomed Opt. 2006;11(2):24015.

23. Zhang HF, Maslov K, Sivaramakrishnan M, Stoica G, Wang LV. Imaging of hemoglobin oxygen saturation variations in single vessels in vivo using photoacoustic microscopy. Appl Phys Lett. 2007;90(5):5–7.
24. Chen Z, Yang S, Xing D. In vivo detection of hemoglobin oxygen saturation and carboxyhemoglobin saturation with multiwavelength photoacoustic microscopy. Opt Lett. 2012; 37(16):3414.
25. Kruger RA, Lam RB, Reinecke DR, Del Rio SP, Doyle RP. Photoacoustic angiography of the breast. Med Phys. 2010;37:6096–100.
26. Deng ZL, Yang XQ, Yu LJ, Gong H. The measurement of hemoglobin oxygen saturation using multi-wavelength photoacoustic microscopy. Saratov Fall Meet 2009 Int Sch Jr Sci Students Opt Laser Phys Biophotonics. 2010;7547.
27. Yao J, Wang L, Yang J-M, Maslov KI, Wong TTW, Li L, et al. High-speed label-free functional photoacoustic microscopy of mouse brain in action. Nat Methods. 2015;12(5):407.
28. Multiparametric spectroscopic photoacoustic imaging of breast cancer development in a transgenic mouse model [Internet]. http://www.thno.org/v04p1062.htm. Accessed 4 Sept 2014.
29. Eustis S, El-Sayed MA. Why gold nanoparticles are more precious than pretty gold: noble metal surface plasmon resonance and its enhancement of the radiative and nonradiative properties of nanocrystals of different shapes. Chem Soc Rev. 2006;35(3):209–17.
30. Jain PK, El-Sayed MA. Universal scaling of plasmon coupling in metal nanostructures: extension from particle pairs to nanoshells. Nano Lett. 2007;7(9):2854–8.
31. Aaron J, Nitin N, Travis K, Kumar S, Collier T, Park SY, et al. Plasmon resonance coupling of metal nanoparticles for molecular imaging of carcinogenesis in vivo. J Biomed Opt. 2007;12(3):34007.
32. Heneweer C, Holland JP, Divilov V, Carlin S, Lewis JS. Magnitude of enhanced permeability and retention effect in tumors with different phenotypes: 89Zr-albumin as a model system. J Nucl Med. 2011;52(4):625–33.
33. Prabhakar U, Maeda H, Jain RK, Sevick-Muraca EM, Zamboni W, Farokhzad OC, et al. Challenges and key considerations of the enhanced permeability and retention effect (EPR) for nanomedicine drug delivery in oncology. Cancer Res. 2013;73(8):2412–7.
34. Maeda H, Wu J, Sawa T, Matsumura Y, Hori K. Tumor vascular permeability and the EPR effect in macromolecular therapeutics: a review. J Control Release. 2000;65(1-2):271–84.
35. Kumar S, Aaron J, Sokolov K. Directional conjugation of antibodies to nanoparticles for synthesis of multiplexed optical contrast agents with both delivery and targeting moieties. Nat Protoc. 2008;3(2):314–20.
36. Hermanson GT. Bioconjugate techniques. Academic Press; 2013. 1200 p.
37. Sardar R, Funston AM, Mulvaney P, Murray RW. Gold nanoparticles: past, present, and future. Langmuir Am Chem Soc. 2009;25(24):13840–51.
38. Häkkinen H. The gold-sulfur interface at the nanoscale. Nat Chem. 2012;4(6):443–55.
39. Harris JM, Chess RB. Effect of pegylation on pharmaceuticals. Nat Rev Drug Discov. 2003;2(3):214–21.
40. Chow A, Brown BD, Merad M. Studying the mononuclear phagocyte system in the molecular age. Nat Rev Immunol. Nature Publishing Group, a division of Macmillan Publishers Limited. All Rights Reserved; 2011;11(11):788–98.
41. Balasubramanian SK, Jittiwat J, Manikandan J, Ong C-N, Yu LE, Ong W-Y. Biodistribution of gold nanoparticles and gene expression changes in the liver and spleen after intravenous administration in rats. Biomaterials. 2010;31(8):2034–42.
42. Sau TK, Murphy CJ. Room temperature, high-yield syntehsis of multiple shapes of gold nanoparticles in aqueous solution. J Am Chem Soc. 2004;126(28):8648–9
43. Nikoobakht B, El-Sayed MA. Preparation and growth mechanism of gold nanorods (NRs) using seed-mediated growth method. Chem Mater. 2003;15(10):1957–62.
44. Dreaden EC, Alkilany AM, Huang X, Murphy CJ, El-Sayed MA. The golden age: gold nanoparticles for biomedicine. Chem Soc Rev. 2012;41(7):2740–79.
45. Turkevich J, Stevenson PC, Hillier J. A study of the nucleation and growth processes in the synthesis of colloidal gold. Discuss Faraday Soc. 1951;11:55.

46. Daniel M-C, Astruc D. Gold nanoparticles: assembly, supramolecular chemistry, quantum-size-related properties, and applications toward biology, catalysis, and nanotechnology. Chem Rev. 2004:293–346.
47. Murphy CJ, Sau TK, Gole AM, Orendorff CJ, Gao J, Gou L, et al. Anisotropic metal nanoparticles: synthesis, assembly, and optical applications. J Phys Chem B. 2005;109(29):13857–70.
48. Jokerst JV, Cole AJ, Van de Sompel D, Gambhir SS. Gold nanorods for ovarian cancer detection with photoacoustic imaging and resection guidance via raman imaging in living mice. ACS Nano. 2012;6(11):10366–77.
49. Zhong J, Wen L, Yang S, Xiang L, Chen Q, Xing D. Imaging-guided high-efficient photoacoustic tumor therapy with targeting gold nanorods. Nanomedicine. 2015;11(6):1499–509.
50. Parker N, Turk MJ, Westrick E, Lewis JD, Low PS, Leamon CP. Folate receptor expression in carcinomas and normal tissues determined by a quantitative radioligand binding assay. Anal Biochem. 2005;338(2):284–93.
51. Zwicke GL, Mansoori GA, Jeffery CJ. Targeting of cancer nanotherapeutics. Nano Rev. 2012;1:1–11.
52. Steinhauser MO, Schmidt M. Destruction of cancer cells by laser-induced shock waves: recent developments in experimental treatments and multiscale computer simulations. Soft Matter. 2014;10(27):4778–88.
53. Zhong J, Yang S. Contrast-enhanced photoacoustic imaging using Indocyanine Green-containing nanoparticles. J Innov Opt Health Sci. 2014;7(1):1350029–1 to 1350029–7.
54. Zhong J, Yang S, Zheng X, Zhou T, Xing D. In vivo photoacoustic therapy with cancer-targeted indocyanine green-containing nanoparticles. Nanomedicine (Lond). 2013;8(6):903–19.
55. Li M-L, Wang JC, Schwartz JA, Gill-Sharp KL, Stoica G, Wang LV. In-vivo photoacoustic microscopy of nanoshell extravasation from solid tumor vasculature. J Biomed Opt. 2009;14(1):010507.
56. Li W, Brown PK, Wang LV, Xia Y. Gold nanocages as contrast agents for photoacoustic imaging. Contrast Media Mol Imaging. 2011;6(January):370–7.
57. Yang X, Skrabalak SE, Li ZY, Xia Y, Wang LV. Photoacoustic tomography of a rat cerebral cortex in vivo with Au nanocages as an optical contrast agent. Nano Lett. 2007;7(12):3798–802.
58. Song KH, Kim C, Cobley CM, Xia Y, Wang LV. Near-infrared gold nanocages as a new class of tracers for photoacoustic sentinel lymph node mapping on a rat model. Nano Lett. 2009;9(1):183–8.
59. Kim C, Cho EC, Chen J, Song KH, Au L, Favazza C, et al. In vivo molecular photoacoustic tomography of melanomas targeted by bioconjugated gold nanocages. ACS Nano. 2010;4(8):4559–64.
60. Liang S, Li C, Zhang C, Chen Y, Xu L, Bao C, et al. CD44v6 monoclonal antibody-conjugated gold nanostars for targeted photoacoustic imaging and plasmonic photothermal therapy of gastric cancer stem-like cells. Theranostics. 2015;5(9):970–84.
61. Mallidi S, Kim S, Karpiouk A, Joshi PP, Sokolov K, Emelianov S. Visualization of molecular composition and functionality of cancer cells using nanoparticle-augmented ultrasound-guided photoacoustics. Photoacoustics. 2015;3(1):26–34.
62. Eckhardt S, Brunetto PS, Gagnon J, Priebe M, Giese B, Fromm KM. Nanobio silver: its interactions with peptides and bacteria, and its uses in medicine. Chem Rev. 2013;113(7):4708–54.
63. Ong C, Lim JZZ, Ng C-T, Li JJ, Yung L-YL, Bay B-H. Silver nanoparticles in cancer: therapeutic efficacy and toxicity. Curr Med Chem. 2013;20(6):772–81.
64. de Lima R, Seabra AB, Durán N. Silver nanoparticles: a brief review of cytotoxicity and genotoxicity of chemically and biogenically synthesized nanoparticles. J Appl Toxicol. 2012;32(11):867–79.
65. Xue C, Metraux GS, Millstone JE, Mirkin CA. Mechanistic study of photomediated triangular silver nanoprism growth. J Am Chem Soc. 2008;130(26):8337–44.
66. Homan KA, Souza M, Truby R, Luke GP, Green C, Vreeland E, et al. Silver nanoplate contrast agents for in vivo molecular photoacoustic imaging. ACS Nano. 2012;6(1):641–50.

67. Homan K, Shah J, Gomez S , Gensler H, Karpiouk A, Brannon-Peppas L , Emelianov S. Combined ultrasound and photoacoustic imaging of pancreatic cancer using nanocage contrast agents. SPIE photons plus ultrasound: imaging and sensing. 2009. p. 71771M.
68. Chen Y-S, Frey W, Kim S, Homan K, Kruizinga P, Sokolov K, et al. Enhanced thermal stability of silica-coated? Gold nanorods for photoacoustic imaging and image-guided therapy. Opt Express. 2010;18(9):8867–78.
69. Dai H. Carbon nanotubes: synthesis, integration, and properties. Acc Chem Res. 2002;35(12): 1035–44.
70. De La Zerda A, Zavaleta C, Keren S, Vaithilingam S, Bodapati S, Liu Z, et al. Carbon nanotubes as photoacoustic molecular imaging agents in living mice. Nat Nanotechnol. 2008;3(9):557–62.
71. Smart SK, Cassady AI, Lu GQ, Martin DJ. The biocompatibility of carbon nanotubes. Carbon. 2006;44(6):1034–47.
72. Nguyen VP, Oh Y, Ha K, Oh J, Kang HW. Enhancement of high-resolution photoacoustic imaging with indocyanine green-conjugated carbon nanotubes. Jpn J Appl Phys. 2015;54(7S1):07HF04.
73. Wilson K, Homan K, Emelianov S. Biomedical photoacoustics beyond thermal expansion using triggered nanodroplet vaporization for contrast-enhanced imaging. Nat Commun. 2012;3:618.
74. Jian J, Liu C, Gong Y, Su L, Zhang B, Wang Z, et al. India ink incorporated multifunctional phase-transition nanodroplets for photoacoustic/ultrasound dual-modality imaging and photoacoustic effect based tumor therapy. Theranostics. 2014;4(10):1026–38.
75. Hannah A, Luke G, Wilson K, Homan K, Emelianov S. Indocyanine green-loaded photoacoustic nanodroplets: dual contrast nanoconstructs for enhanced photoacoustic and ultrasound imaging. ACS Nano. 2014;8(1):250–9.
76. Paproski RJ, Forbrich A, Huynh E, Chen J, Lewis JD. Porphyrin nanodroplets : sub-micrometer ultrasound and photoacoustic contrast imaging agents. Small. 2015:1–10.
77. Huynh E, Leung BYC, Helfield BL, Shakiba M, Gandier J-A, Jin CS, et al. In situ conversion of porphyrin microbubbles to nanoparticles for multimodality imaging. Nat Nanotechnol. 2015;10(4):325–32.
78. Su JL, Wang B, Wilson KE, Bayer CL, Chen Y-S, Kim S, et al. Advances in clinical and biomedical applications of photoacoustic imaging. Expert Opin Med Diagn. 2010;4(6):497–510.
79. Luke GP, Yeager D, Emelianov SY. Biomedical applications of photoacoustic imaging with exogenous contrast agents. Ann Biomed Eng. 2012;40(2):422–37.
80. Mallidi S, Larson T, Aaron J, Sokolov K, Emelianov S. Molecular specific optoacoustic imaging with plasmonic nanoparticles. Opt Express. 2007;15(11):6583–8.
81. Yang X, Stein EW, Ashkenazi S, Wang LV. Nanoparticles for photoacoustic imaging. Wiley Interdiscip Rev Nanomed Nanobiotechnol. 1(4):360–8.
82. Wilson KE, Wang TY, Willmann JK. Acoustic and photoacoustic molecular imaging of cancer. J Nucl Med. 2013;54(11):1851–4.
83. Yang X, Stein EW, Ashkenazi S, Wang LV. Nanoparticles for photoacoustic imaging. Wiley Interdiscip Rev Nanomed Nanobiotechnol. 2009;1(4):360–8.